An Iterative Centroid Approach for Diffeomorphic Online Atlasing

Antoine Legouhy, François Rousseau, Christian Barillot, and Olivier Commowick

Abstract—Online atlasing, i.e., incrementing an atlas with new images as they are acquired, is key when performing studies on very large, or still being gathered, databases. Regular approaches to atlasing however do not focus on this aspect and impose a complete reconstruction of the atlas when adding images. We propose instead a diffeomorphic online atlasing method that allows gradual updates to an atlas. In this iterative centroid approach, we integrate new subjects in the atlas in an iterative manner, gradually moving the centroid of the images towards its final position. This leads to a computationally cheap approach since it only necessitates one additional registration per new subject added. We validate our approach on several experiments with three main goals: 1- to evaluate atlas image quality of the obtained atlases with sharpness and overlap measures, 2- to assess the deviation in terms of transformations with respect to a conventional atlasing method and 3- to compare its computational time with regular approaches of the literature. We demonstrate that the transformations divergence with respect to a state-of-the-art atlas construction method is small and reaches a plateau, that the two construction methods have the same ability to map subject homologous regions onto a common space and produce images of equivalent quality. The computational time of our approach is also drastically reduced for regular updates. Finally, we also present a direct extension of our method to update spatio-temporal atlases, especially useful for developmental studies.

Index Terms— Atlasing, online, iterative centroid.

I. INTRODUCTION

WE REFER by the term atlas an average model of an anatomical region (here the brain) from a geometric (shape) and iconic (image intensity) point of view. It is a key component of many pipelines in medical image processing to create a neutral reference for a considered population for common alignment [11], to segment regions [5], etc. This tool is also crucial to understand brain variability [28] and to compute statistics on populations [32].

The easiest way to construct atlases may seem very simple: one may for example register all images towards a reference image, and then average all images intensities in that common space. This however creates a bias: constructing an atlas towards a reference or another would give different atlases. If registration was perfectly matching images, the resulting atlas would be exactly the reference image in terms of shape when the atlas is supposed to be an average model in terms of intensities and shape. This is not desirable for many applications and therefore two main families of approaches are commonly used to produce a so-called unbiased atlas:

- Template-based approaches [10], [13], [16] require the choice of an initial reference image onto which each subject is registered. The bias toward this first reference is then compensated using the inverse average transformation from the registration. Iterating over this process and taking the average model of the previous iteration as the new reference produces an unbiased atlas.
- Template-free approaches [33] on the other hand do not rely on an initial reference image thus avoiding the introduction of the bias in the first place. They can be subdivided into two categories:
  - Pairwise methods [25], [26]: they require to register each subject towards all the others. From these pairwise registrations, so-called unbiased subjects can be created that are then averaged.
  - Groupwise methods [14], [18], [19]: they propose to directly compute an average model through a groupwise registration of all the subjects simultaneously. In [12], [31] and [34], it was proposed to take advantage of the generative model developed in [1] to embed atlas creation into a Bayesian framework allowing especially to jointly estimate parameters such as the coefficient balancing image similarity and regularization.

Until the 2000s, magnetic resonance imaging (MRI) databases remained fairly modest in size, often limited to a hundred individuals and rarely in open-access. More recently, the size of datasets has grown considerably, boosted in particular

by the search for statistical power and the appetite of machine learning algorithms. Spread over various periods of time, those new large databases offer the opportunity to produce atlases depicting the population variability across the lifespan. The Human Connectome Project Young Adults, the first completed of its kind, is constituted of about 1200 subjects [29]. Various spin-off projects of the same order of magnitude have then been initiated for lifespan development [27] and aging [4]. At an even bigger scale, the UK Biobank study [21] aspires to include up to 100,000 subjects in 2022. In this context, the recruitment process can take several years, researchers may therefore start working on these databases before their completion. This causes two problems. All the above-mentioned methods require a large number of heavy computations (registrations, transformation compositions, etc.) that increases with the number of subjects (linearly or even quadratically for exhaustive pairwise methods). Their computational cost can thus be prohibitive for a large number of subjects. Furthermore, a crucial aspect is that the computational cost of adding new images to the atlas, for example when new images come to enlarge an existing database, is prohibitive. For most methods, the whole atlasing process has to be restarted from scratch to update the atlas. A notable exception is the exhaustive pairwise method that only requires a large number of registrations (e.g. N registrations if adding a single image to an atlas computed from N images). However, since their computational cost is the largest of all methods in the first place, the gain is relatively low and N registrations to add one image is still long. The community therefore needs online atlasing, i.e., methods which make it possible, as opposed to the direct atlasing ones mentioned above, to update an existing atlas with new images as they arrive without having to redo the entire atlas construction process.

We propose a new atlas construction technique that considers the problem from a different perspective. To do so, we start back from the notion of centroid as it is defined for a set of points in a Euclidean space. Following this common formula, [8] noted that it may be reformulated in an iterative series where one point is added at a time. They generalized this formula to surfaces embedded in a Riemannian manifold to propose an iterative and efficient diffeomorphic atlas construction method for surfaces. [22] presented a similar approach for images using B-splines constrained to preserve topology. We propose in this paper a generalization of the iterative diffeomorphic centroid approach to image atlasing, allowing the atlas to be updated gradually as new images are incorporated. The major advantage of this approach is that the integration of a new image to an existing atlas does not impose to build the atlas from scratch. A single registration step is required which makes it computationally efficient. Benefiting from the log-Euclidean framework for diffeomorphisms from [2], the method also allows the construction of a diffeomorphic atlas unbiased up to a linear transformation (rigid or affine at the choosing of the user). We have formerly presented a limited, basic version of this approach in the conference paper available in [17]. Further, we present in Section II-D how to extend the iterative centroid approach to the creation of spatio-temporal (4D) atlases (i.e., a collection of 3D sub-atlases

from cross-sectional data, each at a given timepoint, where the contribution of each subject is modulated by a weight function that accounts for the distance in age to the timepoint). A version to merge atlases allowing more parallel architectures organizing the atlas creation is also presented in Section II-E.

Section II presents the iterative centroid approach, its specificities for image atlasing and the different variants we introduce. We then present in Section III implementation details and experiments to compare the atlasing technique behavior with direct atlasing (here a modified version of the [13] method, developed in [16]). Using a geometric metric we show that the methods diverge from each other as more and more subjects are included, but stay relatively close. We also compare the atlases using an overlap and a sharpness metric; both showing almost identical results between the two approaches. In addition, we evaluated how the ordering of the subjects influences the result. We demonstrate once again similar variations using both methods. Finally, we conducted computational efficiency experiments showing the superiority of our iterative centroid approach when adding new subjects gradually to an existing atlas.

II. METHOD

A. Theoretical Background

Let us consider the registration of two images I and J, i.e., transforming J onto I so that J and I match as much as possible. We denote by $\tilde{J}$ the image J resampled by a transformation $T: I(x) \sim \tilde{J}(x) = J \circ T(x)$, where x are the spatial coordinates. Going further, if we assume that T belongs to a connected Riemannian manifold, we denote by $\gamma(t)$ the geodesic between identity Id and T defined by $\gamma(0) = $ Id and $\gamma(1) = T$. This framework is often named large deformation diffeomorphic metric mapping (LDDMM). In this case, T is defined by a time varying vector field integrated over time (the geodesic γ).

Diffeomorphisms are widely used in non-linear registration because of their interesting properties: differentiability, bijectivity and differentiability of the inverse map. Another framework for diffeomorphisms parametrizes the transformation T between two images by a stationary velocity field (SVF) integrated over time [2]. In this context, diffeomorphisms together with the composition law are given an infinite Lie group structure to which is associated, via logarithm and exponential maps, its Lie algebra. The latter is a vector space where Euclidean operations are well defined [2]. One operation of interest is the power of a diffeomorphism defined as $T^\alpha = \exp(\alpha \log(T))$. T^α corresponds to the value at $t = \alpha$ of $\gamma(t)$, the diffeomorphic path between Id and T such that $\gamma(0) = $ Id and $\gamma(1) = T$. In the following, all non-linear transformations are assumed to be diffeomorphisms parameterized with SVFs as they allow for large diffeomorphic deformations and are more computationally efficient than LDDMM.

The logarithm of diffeomorphisms parameterized by SVFs is computationally very expensive. Several approaches [3], [30] have therefore suggested to perform all computations, especially composition, in the tangent space of the Lie group and use the exponential (much faster) only when image

resampling is needed. This requires a way to compute the representation in the Lie algebra of the composition of two elements of the Lie group without any logarithm computation. The Baker-Campbell-Hausdorff (BCH) formula allows for such an operation through a series of Lie bracket terms. In particular, for two SVFs v and w close enough to 0, the following series converges:

$$\log(\exp(v) \circ \exp(w)) \approx \text{BCH}(v, w) = v + w + \frac{1}{2}[v, w] + \dots \tag{1}$$

where $[v, w](x) = \text{Jac}(v)(x).w(x) - \text{Jac}(w)(x).v(x)$. It has been shown in [3], [30] that the use of the BCH formula is well suited for diffeomorphisms parameterized as SVFs, even though it is not exactly a Lie group due to the infinite dimension aspect. To simplify notations, unless specified otherwise, the composition of two transformations associated to two SVFs v and w is performed via the BCH: $\exp(v) \circ \exp(w) = \exp(\text{BCH}(v, w))$.

B. Iterative Centroid Atlas Construction

In a Euclidean space Ω, the centroid (barycenter) b_n of a set of n points $\{x_1, \dots, x_n\}$ is defined as the point that minimizes the sum of squared Euclidean distances between itself and each point in the set: $b_n = \text{argmin}_{y \in \Omega} \sum_{i=1}^{n} \|y - x_i\|^2$. A direct solution is $\frac{1}{n} \sum_{i=1}^{n} x_i$ but one can also retrieve it through an iterative approach following:

$$\begin{cases} b_1 & x_1 \\ b_{k+1} & \dfrac{k}{k+1} b_k + \dfrac{1}{k+1} x_{k+1} \end{cases} \tag{2}$$

As depicted in [8], one can extend this formulation to the Riemannian case for surfaces by using the generalization of the notion of straight line to geodesics. In that context, the updated centroid b_{k+1} is situated along the geodesic linking b_k and x_{k+1}, at $\frac{1}{k+1}$ times the distance between the two from b_k.

We define our iterative centroid atlasing following the same spirit, but on images and using diffeomorphisms parametrized by SVFs. Thereafter we assume that the registration of an image I onto an atlas A is performed in two steps: first through the estimation of a linear transformation L and then a diffeomorphism T, so that $A \sim I \circ L \circ T$. Generalizing Equation 2 to a set of images $\{I_1, \dots, I_n\}$, we obtain the following update formula:

$$\begin{cases} A_1 & I_1 \\ A_{k+1} & \dfrac{k}{k+1} A_k \circ T_{k+1}^{-\frac{1}{k+1}} + \dfrac{1}{k+1} I_{k+1} \circ L_{k+1} \circ T_{k+1}^{\frac{k}{k+1}} \end{cases} \tag{3}$$

where L_{k+1} and T_{k+1} are respectively the linear and non linear transformations to resample the new image I_{k+1} onto the current atlas A_k. The atlasing scheme is illustrated in Fig. 1. We apply to A_k a transformation located at $\frac{1}{k+1}$ of the distance from the identity to T_{k+1}^{-1} along the diffeomorphic path. We also apply to I_{k+1}, in addition to the linear transformation, a diffeomorphism located at $\frac{k}{k+1}$ of the distance from the identity to T_{k+1} along the transformation path. Also,
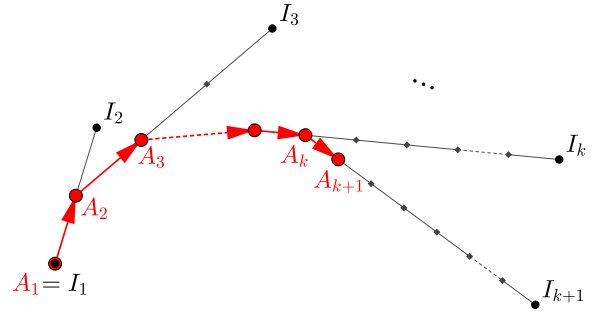

Fig. 1. An illustration of the iterative centroid scheme.

Algorithm 1 Iterative Centroid

1) We register I_{k+1} onto A_k:

$\quad A_k \sim I_{k+1} \circ L_{k+1} \circ T_{k+1}$ (1 registration)

2) For $j = 1, \dots, k$, we update $\Theta_{j,k+1}$ as:

$\quad \Theta_{j,k+1} = \Theta_{j,k} \circ T_{k+1}^{-\frac{1}{k+1}}$ (k BCH)

3) We assign $\Theta_{k+1,k+1} = T_{k+1}^{\frac{k}{k+1}}$

4) Finally we build A_{k+1} as:

$\quad A_{k+1} = \frac{1}{k+1} \sum_{j=1}^{k+1} I_j \circ L_j \circ \Theta_{j,k+1}.$

A_k is made from k images so a weight $\frac{k}{k+1}$ is affected to its intensities whereas I_{k+1} intensities get a weight $\frac{1}{k+1}$. At the end, those two images are transformed and weighted according to their contribution to the atlas.

Now, as opposed to [8] dealing with surfaces, we intend to create an atlas of images. This raises the question of resampling, the images indeed require interpolations on a voxel grid to be reconstructed after undergoing a transformation. This resampling generates blurring effects; it should thus be avoided as much as possible in order to obtain a sharp result, that preserves as much detail as possible. To this end, it is preferable not to use A_k (already a resampled image) when constructing A_{k+1}, but instead to operate on the initial images using transformation compositions such that each image undergoes only one resampling. This is achieved by unravelling Equation 3 such that the sequence (A_k) is expressed only using the initial images $\{I_1, \dots, I_k\}$. The following formulation then emerges:

$$A_{k+1} = \frac{1}{k+1} \left(\sum_{j=1}^{k} \left(I_j \circ L_j \circ \Theta_{j,k} \circ T_{k+1}^{-\frac{1}{k+1}} \right) \right.$$
$$\left. + I_{k+1} \circ L_{k+1} \circ T_{k+1}^{\frac{k}{k+1}} \right) \tag{4}$$

where $\Theta_{j,k}$ is the non-linear part of the transformation bringing I_j onto A_k. To the limit of approximations linked to discretization, the regularity of the transformations is preserved after composition. There are k compositions (using BCH) to perform at iteration k which correspond to the update of the transformations $\Theta_{j,k}$ for $j \leq k$. Algorithm 1 summarizes the process to obtain the new atlas A_{k+1} by adding one image to the current atlas A_k.

We detail two more points to obtain the complete iterative centroid atlas construction method.

1) Initialization: One can start at iteration 1 by initiating $A_1 = I_1$ and $\Theta_{1,1} = \text{Id}$. However, a key point of the method is the possibility to complement an already existing atlas A_p constituted of p images as long as it can be written as $A_p = \frac{1}{p} \sum_{j=1}^{p} I_j \circ L_j \circ T_j$. To do so, we assign $\Theta_{j,p} = T_j, \ \forall j \leq p$.

2) Iterative Procedure: At the end of iteration k we have, for each $j \leq k$, transformations $\Theta_{j,k}$ that map images I_j onto the atlas A_k: $A_k \sim I_j \circ L_j \circ \Theta_{j,k}$. Algorithm 1 is then applied iteratively for all images to add to the initial atlas.

C. Unbiased Atlas Construction

The proposed method, similarly to Guimond *et al.* atlas construction process [13], allows the construction of an atlas unbiased with respect to a linear transformation. So far, we have thus only assumed that the registration produced a linear and a non-linear part. Going in more details, let us now assume that this registration can be written $A \sim I \circ R \circ S \circ D$ where: $R \circ S$ is an affine transformation decomposed into a rigid part R and a stretching part S using polar decomposition (as depicted in [16]), and D is a diffeomorphism.

We can now distinguish two cases:

- By taking $L = R \circ S$ and $T = D$: L encapsulate the entire global part of the overall transformation i.e., rigid and stretching aspects whereas T only account for local displacements. The method will lead - similarly to [13] - to an atlas unbiased up to an affine transformation.
- By taking $L = R$ and $T = S \circ D$: L only consider rigid motion whereas T encapsulate both growth aspects and local displacements. The method will lead to an atlas unbiased up to a rigid transformation. This makes the method eligible for spatio-temporal studies (similarly to [16] for the direct atlasing case). This change to rigid unbiasing will only cost one more composition per image (one BCH), for the composition of S and D.

D. Spatio-Temporal Extension

Our iterative centroid atlas creation method considers by default equal weights for each image. However it is also fully eligible for a spatio-temporal extension where one wants to constitute a series of atlases for a set of specific timepoints. This may be done using weight functions that modulate the contribution of each subject image according to its distance in age to a desired timepoint. These weight functions, often chosen as Gaussian kernels, can have adaptive width [26] to compensate for uneven distribution. A more flexible approach [16] allows in addition to adjust for asymmetric distributions of the ages of the input subjects. Interestingly, and consistently with the relevance of the iterative centroid approach, it is not required to define the weights for all upcoming subjects from the beginning. Only $w_j = K(t_j, t)$, a kernel which tells the unnormalized weight of the image of the jth subject with age t_j for the atlas at timepoint t, has to be known a priori. When a new image arrives, its associated weight can be computed on the fly according to the subjects age through the weight function.

To account for those weights, the formulation is straightforward: it only consists in replacing the occurrences of two terms representing the adjusted weights of the new image and all the previous images. This leads to the following algorithm:

Algorithm 2 Spatio-Temporal Iterative Centroid

---

1) We register I_{k+1} onto A_k:

   $A_k \sim I_{k+1} \circ L_{k+1} \circ T_{k+1}$ (1 registration)

2) We assign $\alpha_{k+1} = \dfrac{w_{k+1}}{\sum_{j=1}^{k+1} w_j}$

3) For $j = 1, \ldots, k$, we update $\Theta_{j,k+1}$ as:

   $\Theta_{j,k+1} = \Theta_{j,k} \circ T_{k+1}^{-\alpha_{k+1}}$ (k BCH)

4) We assign $\Theta_{k+1,k+1} = T_{k+1}^{1-\alpha_{k+1}}$

5) Finally we build A_{k+1} as:

   $A_{k+1} = \dfrac{1}{\sum_{j=1}^{k+1} w_j} \sum_{j=1}^{k+1} w_j I_j \circ L_j \circ \Theta_{j,k+1}$.

Doing so, as a new image arrives, its weight is calculated through the weight function according to the age of the subject. The normalization of the weights is then adjusted to correctly incorporate the new image in the existing atlas.

To properly account for brain development, the transformation T from registrations must embed both the stretching part S (global changes in scaling) and the diffeomorphic part D (local changes): $T = S \circ D$.

E. Merging of Two Atlases, Parallel Extension

Finally, we detail an extension of our method to be executed in parallel when adding more than a few subjects. This relies on the possibility to merge two atlases A_p and $\tilde{A}_q$ made of respectively p and q images and their associated transformations:

$$\begin{cases} A_p: & \{I_1, \ldots, I_p\}, \ \{L_1, \ldots, L_p\}, \ \{\Theta_{1,p}, \ldots, \Theta_{p,p}\} \\ \tilde{A}_q: & \{\tilde{I}_1, \ldots, \tilde{I}_q\}, \ \{\tilde{L}_1, \ldots, \tilde{L}_q\}, \ \{\tilde{\Theta}_{1,q}, \ldots, \tilde{\Theta}_{q,q}\}. \end{cases}$$

These two atlases can be merged into a single one A_{p+q} containing $p + q$ images as follows:

This algorithm is a generalized version of Algorithm 1 (one can retrieve it with $q = 1$). It paves the way for various, more parallel, architectures organizing the atlas creation. In particular, one can organize the atlas creation following a pairwise design as in [9]. The interest of the iterative centroid method is, however, rather to gradually update atlases at a cheap cost rather than directly building an atlas from numerous existing images. For the latter, direct atlasing methods such as the template-based approach [13], [16] are already well adapted.

III. EXPERIMENTS AND RESULTS

In this section, we first showcase an atlas built with (Algorithm 1) and a spatio-temporal one built with (Algorithm 2). We then present a thorough evaluation of the behavior of the core of our method (Algorithm 1). In particular, results found on this core method generalize straightforwardly to the spatio-temporal version (Algorithm 2), especially since

Algorithm 3 Merging of Two Atlases

1) We register $\tilde{A}_q$ onto A_p:
$$A_p \sim \tilde{A}_q \circ L_{p+q} \circ T_{p+q} \qquad \text{(1 registration)}$$

2) For $j = 1, \ldots, p+q$, we update $\Theta_{j,p+q}$ as:
$$\begin{cases} \Theta_{j,p+q} = \Theta_{j,p} \circ T_{p+q}^{-\frac{q}{p+q}}, & \text{for } j \le p \quad (p \text{ BCH}) \\ \Theta_{j,p+q} = \tilde{\Theta}_{j-p,q} \circ T_{p+q}^{\frac{p}{p+q}}, & \text{for } j > p \quad (q \text{ BCH}) \end{cases}$$

3) For $j = 1, \ldots, q$, we assign:
$$I_{p+j} = \tilde{I}_j, \text{ and } L_{p+j} = \tilde{L}_j$$

4) Finally we build A_{p+q} as:
$$A_{p+q} = \frac{1}{p+q} \left(\sum_{j=1}^{p+q} I_j \circ L_j \circ \Theta_{j,p+q} \right)$$

we evaluate the core method unbiased up to a rigid transformation. Moreover, the study of the influence of image ordering detailed in the next sections also indirectly validates the parallel extension of the method (Algorithm 3).

A. MRI Database

Our experiments have been conducted using data from the Human Connectome Project Young Adults[1] database [29] (HCP-YA, age range: 22-35 years old). We have randomly chosen 100 subjects from which we have used the T1-w preprocessed images (brain extraction). The quality of those data is very high: Siemens 3T scan, T1-w 3D MPRAGE, TR: 2400 ms, TE: 2.14 ms, TI: 1000 ms, flip angle: 8°, image dimensions: $260 \times 311 \times 260$, voxel size: $0.7 \times 0.7 \times 0.7$ mm, acquisition time: 7 min 40 sec.

For the spatio-temporal atlas, we used data from the C-MIND database.[2] We selected 197 T1-weighted images of subjects with ages ranging from less than a month to almost 19 years old. It therefore contains brains of different sizes and maturation. In addition, this database has been constituted with more challenging routine clinic acquisitions: Philips 3T scan, T1-w 3D, TR: 8.1 ms, TE: 3.7 ms, TI: 939 ms, flip angle: 8°, image dimensions: $160 \times 256 \times 160$ or $192 \times 192 \times 160$, voxel size: $1 \times 1 \times 1$ mm, acquisition time: 5 min 16 sec.

B. Implementation Details

1) Registration: Our method is agnostic to the registration algorithms used. We have chosen to perform all registrations in two steps using the block matching algorithms from Anima[3]:

- An affine registration with the block-matching algorithm proposed in [7]. This step outputs an affine transformation matrix B that is then decomposed into two parts: a rigid transformation R and a stretching transformation S. This is achieved through polar decomposition (more details in [16]).

[1]Human Connectome Project Young Adults: https://humanconnectome.org/study/hcp-young-adult
[2]C-MIND database, created for the study of normal brain development conducted by Cincinnati Childrens Hospital Medical Center and UCLA and supported by the National Institute of Child Health and Human Development.
[3]Anima: Open source software for medical image processing from the Empenn team. https://anima.irisa.fr - RRID:SCR_017017
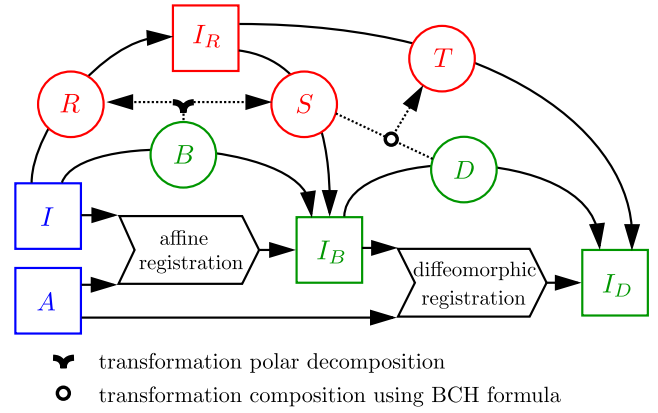

Fig. 2. Illustration of the registrations and operations on transformations. Squares design images whereas circles represent transformations. In blue the initial images (*I* new subject and *A* current atlas), in green the outputs of the registrations (*B* terms for affine, and *D* for diffeomorphic), and in red the components extracted from the operations on the registration transformations.

- A diffeomorphic registration using the algorithm from [6] that directly outputs $\log(D)$ the SVF of the diffeomorphism D linking the two images. This allows to take advantage of the log-Euclidean framework thus avoiding heavy logarithm computations.

We used local (block-wise) squared correlation coefficient as similarity metric. To avoid any bias toward one of the images during the registration of I_{k+1} onto A_k, the similarity metric Sim was computed in an intermediate space between the two images situated at distance $\frac{1}{k+1}$ from A_k along the transformation path: $\text{Sim}\left(A_k \circ T_{k+1}^{-\frac{1}{k+1}}, \; I_{k+1} \circ T_{k+1}^{\frac{k}{k+1}} \right)$.

We have chosen to compute atlases up to a rigid transformation. Therefore, the linear transformation L is rigid: $L = R$ and the non-linear transformation is the combination of stretching and local displacements: $T = S \circ D$. The registration processes and operations on transformations used for our implementation are illustrated in Fig. 2.

2) Transformation Composition: Compositions of two diffeomorphisms are performed on their SVFs using 2nd order BCH. To compose a linear transformation L and a SVF, we first apply $\log(L)$ to the real coordinates of the same image grid as the one of the SVF. This allows to encode the linear transformation into an SVF and then compose it with the non-linear part using 2nd order BCH.

3) Spatio-Temporal Weights: Weights modulating the contribution of each subject for each timepoint of the spatio-temporal atlas have been chosen following the strategy developed in [16]. We chose the following timepoints for constructing the atlas: 1, 1.5, 2, 2.5, 3, 6.5, 10 and 16 years old, and chose an approximate number of 30 subjects per timepoints.

C. Atlas Rendering

We first present an illustration of the atlases produced by our method for visualization purposes. The atlases created by adding one by one the images of the MRI database using Algorithm 1 and above-mentioned processing tools are shown
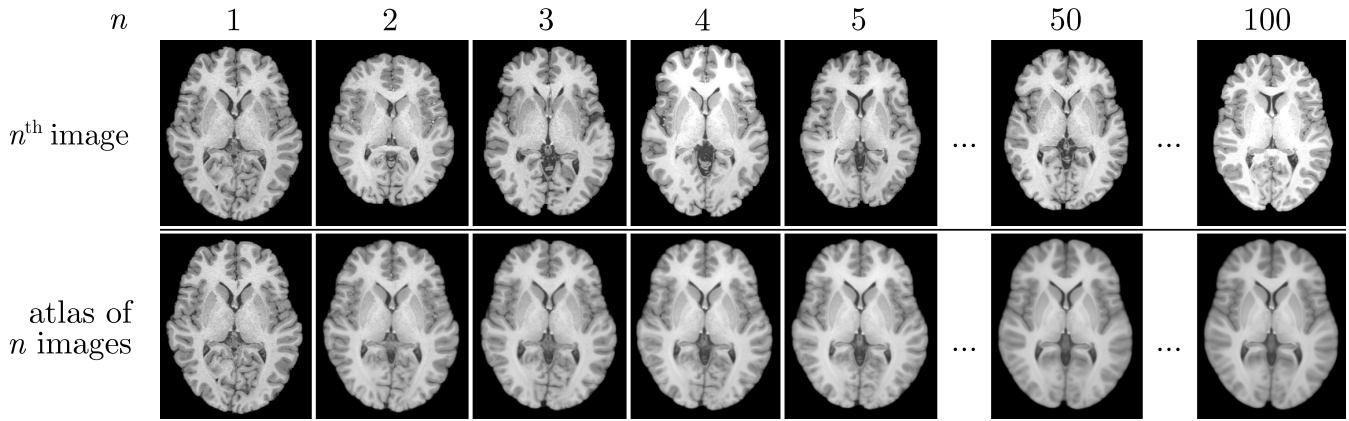
Fig. 3. Resulting consecutive atlases (bottom) obtained through iterative centroid construction as new images (top) are incorporated one by one.

in Fig. 3. The first atlas is obviously identical to the first image. Then one can observe the gradual shift of the centroid that accounts for the new images that are integrated. We obtain at the end an atlas that is an average model of the brain in terms of shape and intensity from the image database of subjects.

We display a spatio-temporal atlas in Fig. 5 i.e., a succession of sub-atlases, each corresponding to a given timepoint between birth and early adulthood, to observe brain development. One can observe a quick general growth, more pronounced along the temporal axis, in the early stages of life until a stabilization around 5 years old. One can also distinguish the myelination process gradually giving its characteristic color to the white matter.

D. Comparison Between Iterative Centroid and Direct Atlasing

We evaluate the results of our approach by comparing its results with a state-of-the-art direct atlasing method: a template-based method proposed in [16] and available as part of Anima scripts.[4] It consists in a natural extension of the method proposed in [13] to handle diffeomorphisms parameterized by SVFs. The same registration and composition algorithms were used, with the same parameters, for both methods.

We have performed, and report in the following three separate experiments to evaluate the behavior of the two methods. The first two experiments start from an atlas built with 50 images using direct atlasing. We then added one by one the 50 other images using our online atlasing. We then compared the results with direct atlases computed with 60, 70, 80, 90 and 100 images. This comparison includes geometric divergence, iconic and overlap measures between the atlases at cortical, sub-cortical and white matter level. We then further evaluated the computational cost of the two methods for two scenarios of atlas creation. Finally, we compared the influence of the ordering in which the images are added for both methods.

[4]Anima-Scripts: Open source scripts using Anima software for medical image processing from the Empenn team. https://anima.irisa.fr - RRID:SCR_017072
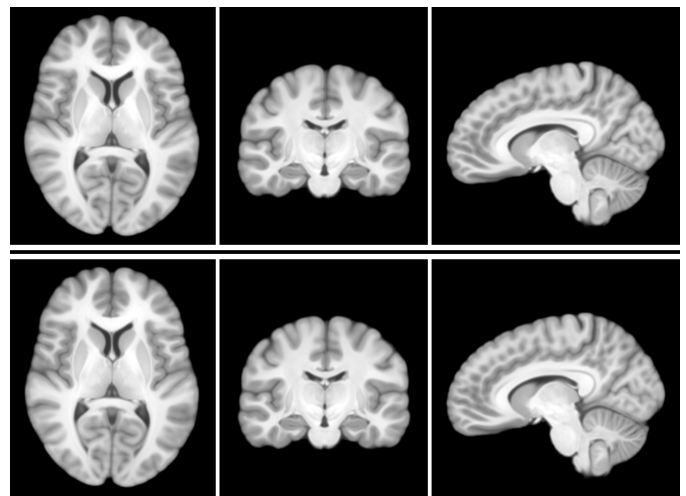

Fig. 4. Atlases of 100 subjects created using the direct atlasing method (top) and the iterative centroid one (bottom).

Both methods output linear transformations L and non-linear transformations Θ mapping each image onto the atlas. We denote by $A_k = \frac{1}{k} \sum_{i=1}^{k} I_j \circ L_j \circ \Theta_{j,k}$ the atlas made of k images using the iterative centroid method and by $\tilde{A}_k = \frac{1}{k} \sum_{i=1}^{k} I_j \circ \tilde{L}_j \circ \tilde{\Theta}_{j,k}$ its counterpart from direct atlasing. Each HCP subject has been segmented using Freesurfer (wmparc) as part of its preprocessing. We grouped the labels by tissue type into 3 sets: sub-cortical, cortical and white matter. They are used as such for the overlap measure. For the geometric divergence and sharpness measures, we fused the labels in each set, and tissue specific results are obtained by weighting metric values by the probability of belonging to this set.

Prior to quantitative assessment, it should be noted that the atlases looks extremely similar. As shown in Fig. 4, even for the atlases with 100 images that are supposed to be the ones accumulating the most divergence, there is barely no difference at all to the naked eye.

1) Geometric Divergence of the Atlases: We first propose to evaluate the divergence between the two atlases A and $\tilde{A}$ by an
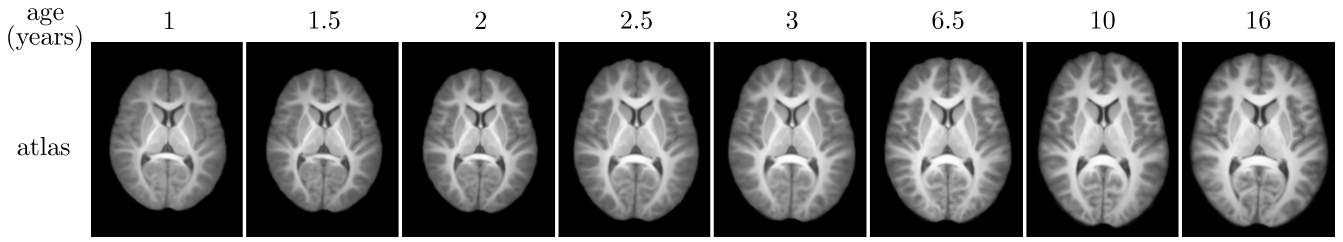
Fig. 5. Spatio-temporal atlas for 8 timepoints between birth and early adulthood showing brain development.
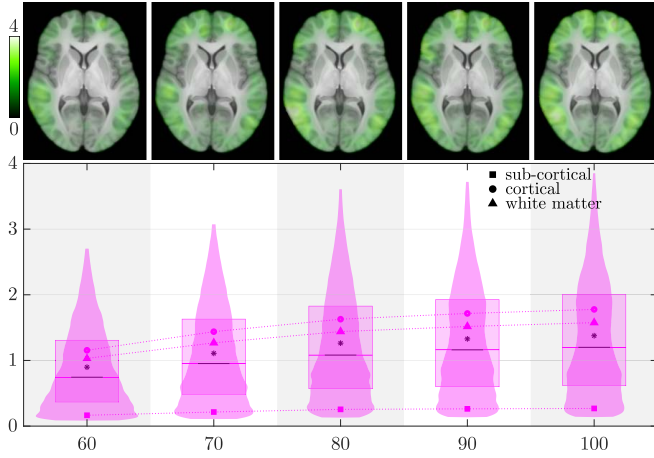

Fig. 6. From left to right atlases with 60, 70, 80, 90 and 100 images. Top: boxplots and violin plots of divergence measure δ (in mm). Bottom: atlases from iterative centroid method overlaid with divergence measure δ (in mm).

Fig. 7. Dice scores associated to sub-cortical (square, left), cortical (disk, center) and white matter (triangle, right) for atlases with 60, 70, 80, 90 and 100 images. Blue: iterative centroid. Red: direct atlasing.

image δ defined from the transformations such that at voxel x:

$$\delta\left(A_k, \tilde{A}_k\right)(x) = \frac{1}{k}\sum_{j=1}^{k}\left\| L_j \circ \Theta_{j,k}(x) - \tilde{L}_j \circ \tilde{\Theta}_{j,k}(x)\right\|_2 \tag{5}$$

This geometrical measurement has the advantage, contrary to most of the iconic ones, of being insensitive to edge issues in image comparison.

In Fig. 6, the evolution of the divergence between the atlases from the two methods with respect to the number of subjects is presented. On the bottom line, quantitative plots suggests that the divergence tends to grow (from a median of 0.74 mm for 60 images, to 1.20 mm for 100) but at a slow and decreasing pace (+0.21 mm between 60 and 70 images but only +0.04 mm between 90 and 100). Despite those numbers that may appear large, there is no noticeable differences between the images to the naked eye (seen Fig. 4. This implies that those differences are most likely related to the vagaries of matching in neighbouring areas of similar contrast. On the top line, the divergence images are superimposed to the atlases from the iterative centroid approach. It reveals that most of the differences are located in outer areas of the brain whereas more central structures are spared.

2) Region Overlap Between the Atlases: We propose to assess the ability of each atlas creation method to properly align the subjects onto a common space by an overlap measure
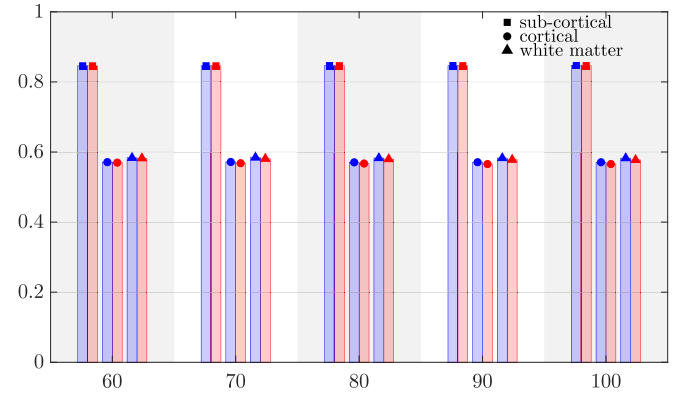
that takes the form of a global Dice score across different labels but also across subjects. This kind of metric has been shown in [24] to be relevant for the validation of registration algorithms and is often used for their evaluation as in [15].

Let Ω_k be the set of all pairs of indices corresponding to the input images for an atlas of k images: $\Omega_k = \{\{i, j\} \in \mathbb{N}^2 \mid i \leq k \text{ and } j < i\}$. We define the global Dice score associated to the atlas A_k as follows:

$$D(A_k) = 2\frac{\displaystyle\sum_{\{i,j\}\in\Omega_k}\sum_{l=1}^{p}|S_{i,l}\circ L_i\circ\Theta_{i,k}\cap S_{j,l}\circ L_j\circ\Theta_{j,k}|}{\displaystyle\sum_{\{i,j\}\in\Omega_k}\sum_{l=1}^{p}\left(|S_{i,l}\circ L_i\circ\Theta_{i,k}| + |S_{j,l}\circ L_j\circ\Theta_{j,k}|\right)} \tag{6}$$

where $|.|$ is the cardinal computed as the number of non-zero voxels, and $S_{i,l}$ corresponds to the label l of the segmentation associated to subject i. Only regions larger than 1000 voxels ($\sim$343 mm^3) were kept. We used this to compute 3 Dice scores associated to the 3 sets of labels (sub-cortical, cortical and white matter) for each atlas.

Dice scores by regions are shown in Fig. 7. Those are almost identical whether using the direct atlasing or the iterative centroid method. Also it is extremely stable with the number of images. In all cases, it reaches a score around 0.85 for sub-cortical areas, 0.57 for cortex and 0.58 for white matter. The relatively low cortical and white matter scores reflect the difficulties of the registration algorithms to exactly perform gyrus-to-gyrus correspondence whereas the good sub-cortical score
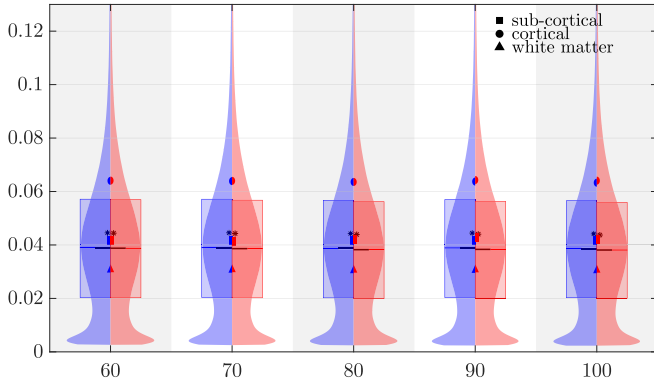
Fig. 8. Boxplots and violin plots of sharpness s for atlases (restrained to the union of the masks) with 60, 70, 80, 90 and 100 images. Blue: iterative centroid. Red: direct atlasing.

method	direct atlasing		iterative centroid
main loop iterations	4	8	
number of non-linear registrations	1200	2400	300
number of BCH computations	1200	2400	45450
indicative processing time (hours)	76.3	152.7	219.8

can be explained by the rather clear boundaries, in anatomical images, of the regions within this set.

3) Sharpness Comparison Between the Atlases: We now present an iconic evaluation to assess the quality of the atlases based on image intensities. Resamplings and registration inaccuracies inherent to the atlas creation process introduce blur. We thus propose in addition a measure of sharpness that quantifies the level of detail of an image. Given $N(x)$, a patch around a voxel x of an image A, we define a local measure of the sharpness s at voxel x as the standard deviation of the patch normalized by its average (the higher the sharpness the better):

$$s(A_k)(x) = \frac{\text{sd}(A_k \circ N(x))}{\text{mean}(A_k \circ N(x))} \tag{7}$$

For this experiment, we chose a patch with a diameter of 5 voxels.

In Fig. 8, quantitative plots of sharpness measurements with respect to the number of images in the atlas are presented. The results shown only account for voxels inside the union of the masks. It appears that the two methods output atlases that are very similar in terms of image quality. The sharpness is almost identical for both and is stable with respect to the number of images. Once again the evolution and values are virtually equal for both atlas construction methods.

Image quality is often a trade-off between sharpness and noise as noisy images can lead to high sharpness measure whereas blurry images may lead to high SNR. However, in the specific context of atlas construction that implies many image averaging and resamplings (voxel averaging) that tend to smooth the result, the impact of noise is rather limited, especially when using a decent number of subjects.

4) Computational Cost: In both compared methods, there are two main sources of time consumption which are the non-linear registrations and the transformation compositions through BCH. As an indication, using a computer with 2×20 cores Intel Xeon Processor E5-2660 v3 2.60GHz, for images of dimension $160 \times 256 \times 190$ ($1 \times 1 \times 1$ mm), it takes about 213 seconds to compute a non-linear registration and 16 seconds to perform a transformation composition through 2nd order BCH.

Let us consider we already have a pre-existing atlas made of k images. We are looking for a measure of the cost of completing this atlas with new images so that it contains a total of $n > k$ images. We have compared the two options evaluated earlier to perform this task:

- **Direct method:** Whatever the previous atlas, the new one has to be built from scratch. Let p be the number of iterations of the main loop. The method requires pn non-linear registrations and pn transformation compositions. The latter compositions are done through BCH and correspond to the composition of the affine and the non-linear transformations from the registrations (only for an atlas up to a rigid transformation).
- **Iterative centroid method:** Using the pre-existing atlas, the method requires $n - k$ non-linear registrations and $(n-k)+\sum_{i=k+1}^{n} i = \frac{1}{2}(n-k)(n+k+3)$ transformations compositions through BCH. The first part corresponds to the composition of the affine and the non-linear transformations from the registrations. The second part corresponds to the update of the Θ transformations (only for an atlas up to a rigid transformation).

Now we showcase two scenarios that give an idea of the strengths and weaknesses of both methods in terms of computational cost.

a) Atlasing from 300 images: We already have in our possession 300 images and we want to build an atlas from it. The amount of non-linear registrations and BCH computations and an indicative processing time for both methods necessary to build this atlas are presented in Table I.

In this configuration, where a single atlas is built from scratch, direct atlasing is the best suited method with direct atlasing requiring 153 hours and online atlasing 220 hours.

b) Atlasing by adding images: We now have a pre-existing atlas made of 200 images and, acquisitions being gathered gradually, we want to update this atlas every 10 new images until we have a final amount of 300. The amount of non-linear registrations and BCH computations as well as an indicative processing time for both methods necessary to update the previous atlas is presented in Fig. 9.

In this configuration, where an atlas in updated gradually as new images arrive, iterative centroid is the best suited method. Indeed, updates take only from 9.77 hours at first step to 13.77 at the last (+0.44 hours at each step) for iterative centroid. In comparison, even for only 4 main loop iterations
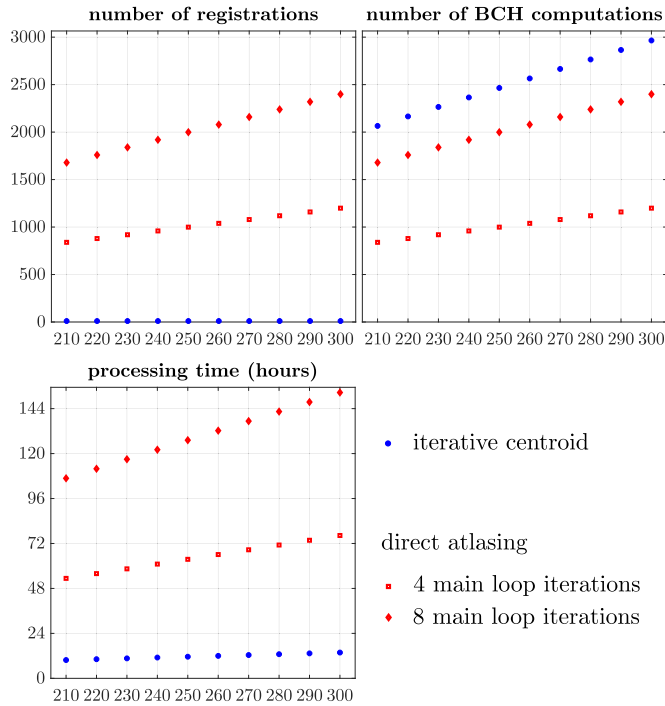
Fig. 9. Number of non-linear registrations, number of BCH computations and indicative processing time to update the atlas at each step (every 10 new images from 200 to 300) using iterative centroid and a direct atlasing. Abscissa represents the number of images of the atlas at each step.

Fig. 10. Divergence δ (in mm) of atlases with shuffled orderings compared to the one with the reference ordering for both template-based and iterative centroid methods. Boxplots only account for the ten totally random combinations (gray).

(which is not much), it takes from 53.37 hours for the first step to 76.27 hours for the last ($+2.54$ hours at each step) for the direct atlasing method.

To sum up, in terms of computational cost, direct atlasing shows better results when it comes to build a single atlas from scratch. On the other hand, the iterative centroid method performs better in case of an atlas being updated gradually. The more images there are in total and the shorter the steps are, the better iterative centroid behaves compared to its direct counterpart.

5) Influence of the Ordering: This experiment is designed to evaluate the influence on the result of the order in which the images are introduced, in particular to apprehend a potential bias towards the first image.

To evaluate the influence of the image ordering for both atlas creation methods, we have chosen a given ordering as reference and compared the results to the ones obtained with other orderings. The comparison was made using the same divergence measure as in Section III-D.1, and the iterative centroid version follows Algorithm 1. For this experiment, we have built atlases made of ten images, the reference ordering is thereupon characterized by the list $(1, 2, 3, 4, 5, 6, 7, 8, 9, 10)$. The set of shuffled orderings for this experiment includes:

- 2 favorable cases:
  - Same ordering except for a permutation of the 5th and 6th (dark green).
  - Same ordering for the first five then random ordering of the rest (light green).
- The least favorable case: reverse ordering (red).
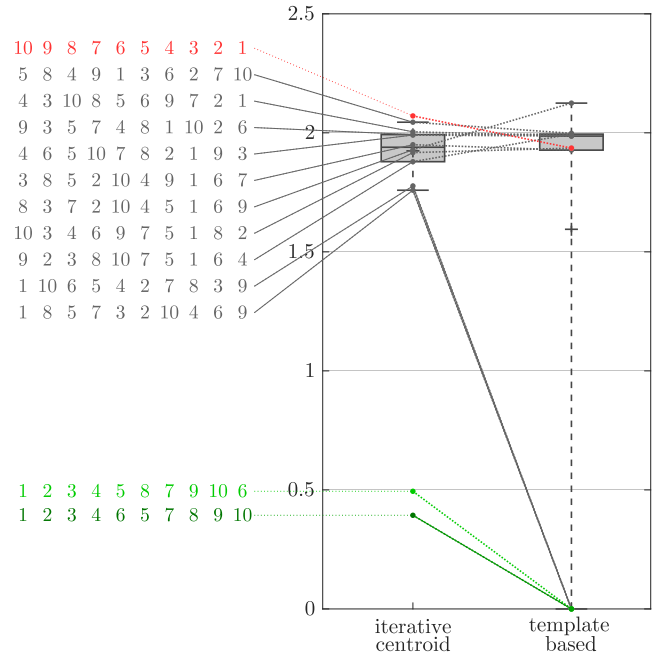- 10 entirely random combinations (gray).

Results are shown in Fig. 10. For the template-based method, only the first image, which is the initial reference, has an influence on the divergence. Given that, if the first element of the ordering is the same as the reference ordering, the divergence is zero. If not, both template-based and iterative centroid approaches show comparable results. For the latter, having a favorable ordering (same beginning as the reference) leads to a much smaller divergence.

This experiment indicates that, using the iterative centroid method, the order in which the images are introduced has a slight influence on the result. However, this tendency remains in similar proportions to the direct atlasing method.

IV. DISCUSSION

In our implementation, diffeomorphisms are parametrized by SVFs, which do not allow the coverage of the whole set of diffeomorphisms. Although this approach is widely used thanks to the convenience of its infinite-dimensional Lie group structure, one might consider a more exhaustive LDDMM parametrization based on time varying velocity fields.

We have used transformation compositions through BCH formula to ensure that only one resampling by subject is necessary, thus providing a sharper result. However, geometric inaccuracies linked to composition approximation through BCH and discretization are likely to accumulate. The BCH approximation was used to bypass the heavy computation of diffeomorphism logarithms when composing transformations. One can imagine a more accurate yet way slower version of the same iterative centroid approach without this shortcut, using logarithm computations instead (although their computation through scaling and squaring are also approximations).

It is likely that part of the observed divergence is linked to BCH approximations. Those are widely used in computational anatomy whenever the SVF framework is involved. A technical note detailing its convergence and the way errors can accumulate with respect to the voxel size, number of composition and approximation order would be of best interest to the community.

We have presented a rather generic recipe which can easily be adapted. The present implementation does not specifically follow the generative model from [1]. However, the general method is not incompatible with it since the iterative centroid approach perfectly accommodates the assumption that images are generated from the latent atlas. Bayesian iterative centroid implementations are possible, analogous to the Bayesian groupwise ones like [34].

When reconstructing an image I' from an image I after a deformation T, to account for signal accumulation in contractions and signal dilution in expansion, an intensity modulation like using the Jacobian determinant of the transformation J_T should be performed: $I'(x) = J_T(x) \cdot I \circ T(x)$. This Jacobian weight terms naturally pops in when deriving the equations in the Bayesian formulation in [20]. This has not been explicitly displayed in the equations but should be considered if needed.

In this paper we used the local squared correlation coefficient as similarity metric because of its versatility. It allows the matching of images of different contrast which is crucial when dealing with still developing brains for example. For a contrast-homogeneous population, one might prefer the sum of squared differences over the whole images. In that case, the above mentioned intensity modulation has importance.

We have proposed the sharpness as a measure of image quality of the resulting atlases. However, image quality is often a trade-off between sharpness and noise, as noisy images can lead to high sharpness whereas blurry images lead to lower noise. Yet, in the specific context of atlases, we believe that the danger comes mainly from the sharpness. Indeed, the construction of an atlas involves a lot of image averaging and resampling (voxel averaging) which tends to smooth the result rather than to induce noise. With a decent number of subjects, the impact of noise quickly fades.

V. Conclusion

We have proposed a novel online atlas construction method based on an iterative centroid process. It allows the gradual incorporation of new images into a pre-existing atlas at a low computational cost: the image is added to the atlas without having to restart the whole atlas construction process. This approach thus only necessitates one registration per new image. It has been used to produce an atlas of 100 images. We derived from it a construction method producing an atlas unbiased up to either an affine or a rigid transformation. The methods proposed in the paper are made available open source in Anima scripts.[5] We have also introduced a second algorithm that extends this online method to spatio-temporal atlasing

[5]Anima-Scripts: Open source scripts using Anima software for medical image processing from the Empenn team.
https://anima.irisa.fr - RRID:SCR_017072

using a predefined weight kernel. Finally a third algorithm, generalization of the first, was presented for merging two atlases, unlocking more parallel architectures.

We produced two types of atlases: single timepoint ones base on Algorithm 1 using HCP young adult high quality data, and a spatio-temporal one based on Algorithm 2 using routine clinic C-MIND pediatric data to highlight brain development.

We have performed numerous experiments in order to compare the iterative centroid approach to a direct atlasing one using the same registration and composition tools. It led to the conclusion that:

- There is barely no differences at all to the naked eye between the results of the two approaches.
- The divergence between both methods is small, localized in cortical areas and tends to grow but at a slow and decreasing pace with the addition of images.
- Both methods show the same ability to overlap regions across subjects composing the atlas.
- The obtained atlases from both approaches have shown no differences in terms of image sharpness.
- In terms of computational cost, direct atlasing is more advantageous to build a large atlas from scratch, whereas the iterative centroid method prevails for gradual updates of an existing one.
- The influence of the ordering of the subjects is similar for both methods.

The trend being at large, growing databases, the proposed online atlasing method offers an interesting tool to update an atlas at reasonable computational cost as new images arrive. Future work will further study how to incorporate images that have a longitudinal component, i.e., images of the same subject over time to build a longitudinal atlas, as opposed to the cross-sectional atlasing method proposed in this paper.

References

[1] S. Allassonnière, Y. Amit, and A. Trouvé, "Towards a coherent statistical framework for dense deformable template estimation," *J. Roy. Stat. Soc. B, Stat. Methodol.*, vol. 69, no. 1, pp. 3–29, Jan. 2007.

[2] V. Arsigny, O. Commowick, X. Pennec, and N. Ayache, "A log-Euclidean framework for statistics on diffeomorphisms," in *Proc. MICCAI*, vol. 4190, 2006, pp. 924–931.

[3] M. Bossa, M. Hernandez, and S. Olmos, "Contributions to 3D diffeomorphic atlas estimation: Application to brain images," in *Medical Image Computing and Computer-Assisted Intervention MICCAI 2007* (Lecture Notes in Computer Science), vol. 4791. Berlin, Germany: Springer, 2007, pp. 667–674.

[4] S. Y. Bookheimer *et al.*, "The lifespan human connectome project in aging: An overview," *NeuroImage*, vol. 185, pp. 335–348, Oct. 2019.

[5] M. Cabezas, A. Oliver, X. Lladó, J. Freixenet, and M. Bach Cuadra, "A review of atlas-based segmentation for magnetic resonance brain images," *Comput. Methods Programs Biomed.*, vol. 104, no. 3, pp. e158–e177, Dec. 2011.

[6] O. Commowick, N. Wiest-Daesslé, and S. Prima, "Automated diffeomorphic registration of anatomical structures with rigid parts: Application to dynamic cervical MRI," in *Proc. 15th Int. Conf. Med. Image Comput. Comput. Assist. Intervent*, vol. 15, no. 2, 2012, pp. 163–170.

[7] O. Commowick, N. Wiest-Daessle, and S. Prima, "Block-matching strategies for rigid registration of multimodal medical images," in *Proc. 9th IEEE Int. Symp. Biomed. Imag. (ISBI)*, May 2012, pp. 700–703.

[8] C. Cury, J. A. Glaunès, and O. Colliot, "Diffeomorphic iterative centroid methods for template estimation on large datasets," in *Geometric Theory of Information*, vol. 10. Berlin, Germany: Springer, 2014, pp. 273–299.

[9] C. Cury *et al.*, "Statistical shape analysis of large datasets based on diffeomorphic iterative centroids," *Frontiers Neurosci.*, vol. 12, pp. 1–18, Nov. 2018.

[10] V. Fonov *et al.*, "Unbiased average age-appropriate atlases for pediatric studies," *NeuroImage*, vol. 54, no. 1, p. 313—327, 2011.

[11] A. Gholipour, N. Kehtarnavaz, R. Briggs, M. Devous, and K. Gopinath, "Brain functional localization: A survey of image registration techniques," *IEEE Trans. Med. Imag.*, vol. 26, no. 4, pp. 427–451, Apr. 2007.

[12] P. Gori, O. Colliot, Y. Worbe, L. Marrakchi-Kacem, and S. Lecomte, "Bayesian atlas estimation for the variability analysis of shape complexes," in *Medical Image Computing and Computer Assisted Intervention*. Berlin, Germany: Springer, 2013, pp. 267–274.

[13] A. Guimond, J. Meunier, and J.-P. Thirion, "Average brain models: A convergence study," *Comput. Vis. Image Understand.*, vol. 77, no. 2, pp. 192–210, Feb. 2000.

[14] S. Joshi, B. Davis, M. Jomier, and G. Gerig, "Unbiased diffeomorphic atlas construction for computational anatomy," *NeuroImage*, vol. 23, pp. S151–S160, Jan. 2004.

[15] A. Klein *et al.*, "Evaluation of 14 nonlinear deformation algorithms applied to human brain MRI registration," *NeuroImage*, vol. 46, no. 3, pp. 786–802, Jul. 2009.

[16] A. Legouhy, O. Commowick, F. Rousseau, and C. Barillot, "Unbiased longitudinal brain atlas creation using robust linear registration and log-Euclidean framework for diffeomorphisms," in *Proc. IEEE 16th Int. Symp. Biomed. Imag. (ISBI)*, Apr. 2019, pp. 1038–1041.

[17] A. Legouhy, O. Commowick, F. Rousseau, and C. Barillot, "Online atlasing using an iterative centroid," in *Proc. Int. Conf. Med. Image Comput. Comput.-Assist. Intervent.*, Cham, Switzerland: Springer, 2020, pp. 366–374.

[18] P. Lorenzen, B. Davis, G. Gerig, E. B. Bullitt, and S. Joshi, "Multiclass posterior atlas formation via unbiased Kullback–Leibler template estimation," in *Medical Image Computing and Computer-Assisted Intervention—MICCAI*, 2004, pp. 95–102.

[19] P. Lorenzen, C. Brad Davis, and S. Joshi, "Unbiased atlas formation via large deformations metric mapping," in *Medical Image Computing and Computer-Assisted Intervention—MICCAI*. Berlin, Germany: Springer, 2005, pp. 411–418.

[20] J. Ma, I. M. Miller, A. Trouvé, and L. Younes, "Bayesian template estimation in computational anatomy," *NeuroImage*, vol. 35, no. 1, pp. 27–32, 2014.

[21] K. L. Miller *et al.*, "Multimodal population brain imaging in the U. K. Biobank prospective epidemiological study," *Nature Meurosci.*, vol. 19, pp. 1523–1536, Sep. 2016.

[22] V. Noblet, C. Heinrich, F. Heitz, and J.-P. Armspach, "An efficient incremental strategy for constrained groupwise registration based on symmetric pairwise registration," *Pattern Recognit. Lett.*, vol. 33, no. 3, pp. 283–290, Feb. 2012.

[23] T. Rohlfing, N. M. Zahr, E. V. Sullivan, and A. Pfefferbaum, "The SRI24 multichannel atlas of normal adult human brain structure," *Human Brain Mapping*, vol. 31, no. 5, pp. 798–819, Dec. 2009.

[24] T. Rohlfing, "Image similarity and tissue overlaps as surrogates for image registration accuracy: Widely used but unreliable," *IEEE Trans. Med. Imag.*, vol. 31, no. 2, pp. 153–163, Feb. 2012.

[25] D. Seghers, E. D'Agostino, F. Maes, D. Vandermeulen, and P. Suetens, "Construction of a brain template from MR images using state-of-the-art registration and segmentation techniques," in *Proc. MICCAI*, vol. 9, 2004, pp. 696–703.

[26] A. Serag *et al.*, "Construction of a consistent high-definition spatiotemporal atlas of the developing brain using adaptive kernel regression," *NeuroImage*, vol. 59, no. 3, pp. 2255–2265, Feb. 2012.

[27] L. H. Somerville *et al.*, "The lifespan human connectome project in development: A large-scale study of brain connectivity development in 5–21 year olds," *NeuroImage*, vol. 183, pp. 456–468, Dec. 2018.

[28] A. W. Toga, P. M. Thompson, M. S. Mega, K. L. Narr, and R. E. Blanton, "Probabilistic approaches for atlasing normal and disease-specific brain variability," *Anatomy Embryol.*, vol. 204, no. 4, pp. 267–282, Oct. 2001.

[29] D. C. Van Essen *et al.*, "The human connectome project: A data acquisition perspective," *Neuroimage*, vol. 62, no. 4, pp. 2222–2231, Oct. 2012.

[30] T. Vercauteren, X. Pennec, A. Perchant, and N. Ayache, "Symmetric log-domain diffeomorphic registration: A demons-based approach," in *Medical Image Computing and Computer Assisted Intervention*. Berlin, Germany: Springer, 2008, pp. 754–761.

[31] J. Wang and M. Zhang, "Bayesian atlas building with hierarchical priors for subject-specific regularization," in *Medical Image Computing and Computer Assisted Intervention*, vol. 12904. Berlin, Germany: Springer, 2021.

[32] B. Whitcher, J. J. Wisco, N. Hadjikhani, and D. S. Tuch, "Statistical group comparison of diffusion tensors via multivariate hypothesis testing," *Magn. Reson. Med.*, vol. 57, no. 6, pp. 1065–1074, 2007.

[33] G. Wu, H. Jia, Q. Wang, F. Shi, P.-T. Yap, and D. Shen, "Emergence of groupwise registration in MR brain study," in *Biosignal Processing: Principles and Practices*. Boca Raton, FL, USA: Taylor & Francis, 2012.

[34] M. Zhang, N. Singh, and P. Fletcher, "Bayesian estimation of regularization and atlas building in diffeomorphic image registration," in *Proc. IPMI*, 2013, pp. 37–48.